Superlattice Dislocations in L12 Ordered Alloys and in Alloys Containing L12 Ordered Precipitates

Hosson, J.T.M. De

Published in:
Materials Science and Engineering

DOI:
10.1016/0025-5416(86)90288-0

Publication date:
1986

Materials Science and Engineering, 81 (1986) 515-523

Superlattice Dislocations in $L1_2$ Ordered Alloys and in Alloys Containing $L1_2$ Ordered Precipitates

J. T. M. DE HOSSON

Department of Applied Physics, Materials Science Centre, University of Groningen, Nijenborgh 18, 9747 AG Groningen (The Netherlands)

(Received November 22, 1985)

ABSTRACT

In this paper we report the dislocation configurations in $L1_2$ ordered alloys and in alloys containing $L1_2$ ordered precipitates. The alloy system Cu-Ni-Zn was chosen because, in the ordered alloy Cu_2NiZn, two structures ($L1_0$ and $L1_2$) are possible and these influence the mechanical behaviour. A rather random distribution of superlattice dislocations and superlattice dislocation dipoles is observed in the $L1_2$ ordered system, whereas planar dislocation arrays such as pile-ups and multipoles are present in the disordered alloy. Configurations of superdislocation dipoles and of superlattice dislocations on {111} were calculated and compared with transmission electron microscopy observations. Superlattice dislocation configurations on {111} and {100} planes were observed in nickel-base superalloys containing $L1_2$ ordered precipitates.

1. INTRODUCTION

The problem of understanding the dislocation microstructure in ordered alloys has a long history. The dislocation concept introduces problems as applied to intermetallic compounds, because a unit dislocation attempting to glide through an ordered lattice should experience a large resistance due to the creation of disorder across the glide plane behind the gliding dislocation, which was in contrast with experimental observations. Koehler and Seitz [1] argued that the large resistance might be ruled out if dislocations in ordered alloys were to be paired such that the order destroyed by the leading dislocation would be immediately restored by the trailing dislocation. Dehlinger and Graf [2] pointed out that, since nucleation of order should occur randomly within a grain, narrow regions of disorder would remain after impingement of ordered regions which were "out of step" with one another (the so-called antiphase boundaries (APBs)).

Using transmission electron microscopy (TEM), Ogawa *et al.* [3] revealed APBs for the first time, whereas the paired dislocation, *i.e.* the superlattice dislocation, was first imaged by Marcinkowski *et al.* [4]. Detailed interpretations of such micrographs were greatly facilitated by the development of the theory of dynamic electron diffraction.

It has been observed that the formation of long-range order in alloys results in a marked change in their mechanical properties. For instance, some $L1_2$ ordered alloys (*e.g.* Ni_3Al) exhibit an increase in flow stress with increasing deformation temperature, whereas their disordered configurations show a substantial decrease in flow stress. In this paper we report the dislocation configurations in $L1_2$ ordered alloys (Cu_2NiZn) and in alloys containing $L1_2$ ordered precipitates (nickel-base superalloys). Configurations of superlattice dislocations and superlattice dislocation dipoles were calculated and compared with TEM observations.

2. MATERIALS

2.1. $L1_2$ ordered alloy

Physical properties of Cu-Ni-Zn alloys with a composition in the neighbourhood of Cu_2NiZn exhibit an anomalous behaviour (for a review see ref. 5). Recently, we determined the long-range zinc ordering S'' in Cu_2NiZn as a function of the annealing temperature by single-crystal neutron diffraction [6]. The long-range order parameter S'' is

0025-5416/86/$3.50

obtained by taking the measured intensities of the superreflections relative to the corresponding intensities of the fundamental reflections and averaging over equivalent reflections [7]. From the single-crystal neutron diffraction study we concluded that, below the first critical temperature T_{c1} of about 774 K, a modified $L1_2$ structure exists, in which zinc atoms occupy one of the four interpenetrating single cubic sublattices while copper and nickel are still randomly distributed over the remaining three sublattices. Below a second critical temperature T_{c2} of about 598 K, a modified $L1_0$ structure exists, in which the copper and nickel atoms each occupy their own sublattice ($S' = 1$). Single crystals of Cu_2NiZn were grown by the strain anneal method, which produced small but very good crystals with respect to homogeneity.

2.2. Nickel-base superalloy containing $L1_2$ ordered precipitates

The chemical composition of the nickel-base superalloy is 14.92 wt.% Cr, 16.62 wt.% Co, 4.95 wt.% Mo, 3.70 wt.% Al, 3.54 wt.% Ti, 0.024 wt.% C, 0.023 wt.% B, 55.99 wt.% Ni and 0.24 wt.% of other elements. The argon-atomized powders are hot isostatically pressed at 1130 °C and 1 kbar for 6 h. After spark erosion the specimens were given the following heat treatment: 4 h at 1110 °C followed by an oil quench; 24 h at 650 °C followed by an air quench; 8 h at 760 °C followed by an air quench. The grain size in the hot isostatically pressed condition is 10–20 μm. The matrix is hardened by 48 vol.% γ' $L1_2$ ordered precipitates, which can be divided into three groups: (a) cuboids with an edge length of 1–4 μm, along the grain boundaries and groups of eight in the matrix; (b) cuboids with an edge length of 100–200 nm; (c) spherical particles with a diameter of 50–60 nm.

3. SUPERLATTICE DISLOCATIONS AND SUPERLATTICE DISLOCATION DIPOLES IN $L1_2$ ORDERED STRUCTURES

3.1. Configurations of superlattice dislocations and superlattice dislocation dipoles

Glide of a unit dislocation with a Burgers vector $\frac{1}{2}\langle 110\rangle$ in an $L1_2$ ordered structure results in the production of an APB in its wake. A second dislocation, having the same Burgers vector, gliding in the same slip plane will cancel the APB produced by the first dislocation. This configuration is shown schematically in Fig. 1(a). It is well known that in f.c.c. materials a unit dislocation can split into two Shockley partials with Burgers vectors of the type $\frac{1}{6}\langle 211\rangle$ separated by a stacking fault. The splitting may also occur in the $L1_2$ ordered structure (see Fig. 1(b)). A third dissociation scheme of a superlattice dislocation is shown in Fig. 1(c), where a superlattice intrinsic stacking fault is bounded by two superlattice Shockley partials, having a Burgers vector of the type $\frac{1}{3}\langle 211\rangle$. This dissociation scheme is expected to occur only in ordered structures with a very large APB energy and a relatively low superlattice intrinsic stacking fault energy. Each superlattice Shockley partial might split into three ordinary Shockley partials separated by a complex stacking fault and an APB as illustrated in Fig. 1(d). However, the very high APB energy (at least a hundred times larger than the superlattice intrinsic stacking fault energy), which is necessary to make the dissociation in Fig. 1(d) more favourable than those in Figs. 1(a) and 1(b) [8], results in a self-energy of the sixfold dissociation larger than the self-energy of the twofold dissociation in Fig. 1(c). Hence, the existence of dissociation as in Fig. 1(d) is very unlikely [8, 9].

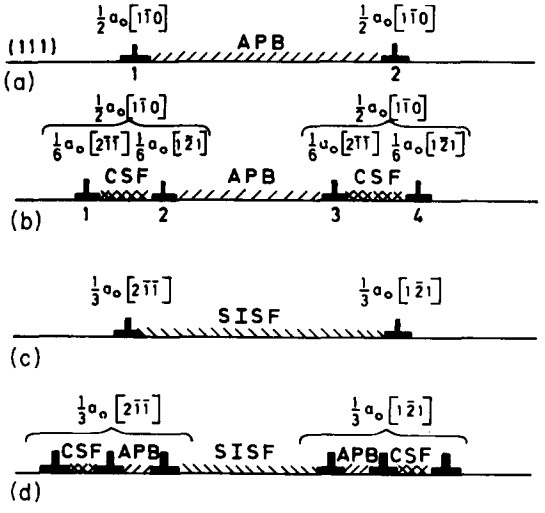

Fig. 1. Possible dissociation schemes of a superlattice dislocation on the (111) plane in the $L1_2$ structure (CSF, complex stacking fault; APB, antiphase boundary; SISF, superlattice intrinsic stacking fault).

Since the critical temperature for ordering of the alloy Cu_2NiZn is not high, it can be expected that its APB energy is not large and hence the dissociation scheme according to Fig. 1(b) is assumed to occur. This is in contrast with $L1_2$ ordered Ni_3Al which shows a high critical temperature for ordering and consequently a high APB energy. Whether the dissociation scheme in Figs. 1(a) and 1(b) or that in Fig. 1(c) occurs is dependent on the relative values of the APB energy and the superlattice intrinsic stacking fault energy.

When two superlattice dislocations of opposite signs gliding on parallel slip planes come close to each other, they can form a so-called superlattice dislocation dipole. The activation of two Frank–Read sources on parallel planes may result in the formation of unit dislocation dipoles or multipoles in f.c.c. metals and disordered solid solutions. Similarly, two Frank–Read sources in an ordered alloy may lead to the formation of superlattice dislocation dipoles. However, they can also be formed at a sessile superjog on a moving superlattice dislocation as illustrated in Fig. 2. The sessile superjog cannot glide in a conservative way as the glissile superlattice dislocation does under an applied stress. Therefore, superlattice dislocation dipoles are left in the wake of moving superlattice dislocations containing superjogs. These superjogs are of the type discussed by Vidoz and Brown [23] which can develop tubular APBs.

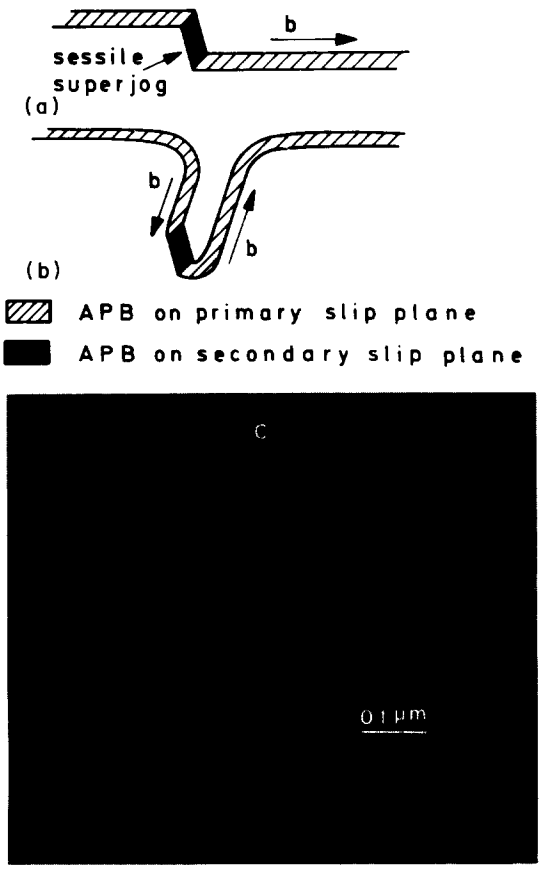

Fig. 2. Jog mechanism of the superlattice dislocation dipole formation: (a) superlattice dislocation containing a super jog in the unstressed state; (b) bowing-out of the glissile parts under the applied stress; (c) situation (b) observed by TEM.

3.2. Theoretical considerations about the separation of the Shockley partials

The total energy for each dissociation in Fig. 1 can be calculated in order to see which is the most favourable in the ordered $L1_2$ structure. Suzuki *et al.* [9] compared the dissociation in Fig. 1(a) with that in Fig. 1(c) using the isotropic elasticity theory, taking into account the fault energies, the self-energies and the interaction energies of the dislocations. The following criteria for the total energy of both dislocation schemes, E_a and E_c respectively, can be derived:

$$\frac{E_{APB}}{E_{SISF}} \lesseqgtr 1.9\,\frac{d_s}{b} \leftrightarrow E_a \lesseqgtr E_c \qquad (1)$$

for a screw superlattice dislocation and

$$\frac{E_{APB}}{E_{SISF}} \lesseqgtr 1.1\left(\frac{d_e}{b}\right)^{2/7} \leftrightarrow E_a \lesseqgtr E_c \qquad (2)$$

for an edge superlattice dislocation, where d_s is the separation of the two unit dislocations (constituting a screw superlattice dislocation for the scheme described in Fig. 1), d_e is the corresponding separation in an edge superlattice dislocation and b is the Burgers vector of the unit dislocation.

Theoretical values for E_{APB} in Cu_2NiZn of about 80 mJ m^{-2} and for d_s and d_e of 5.1 nm and 9.6 nm respectively have been calculated by de Groot *et al.* [10]. The stacking fault energy is 35 mJ m^{-2} [11] and the lattice parameter is equal to 0 3634 nm. Substituting these values in eqns. (1) and (2) results in an energy for the dissociation scheme in Fig. 1(a) which is less than for the scheme in Fig. 1(c) for both the screw and the edge superlattice dislocation. Hence, the dissociation scheme in Fig. 1(c) is not expected to occur in Cu_2NiZn.

To distinguish between the twofold dissociation (the scheme in Fig. 1(a)) and the four-

fold dissociation (the scheme in Fig. 1(b)) of the superlattice dislocation, anisotropic elasticity theory is used to calculate the total energy of both configurations (E_a and E_b respectively):

$$E_a = C_\theta\left\{\ln\left(\frac{R}{\epsilon_a}\right) + \ln\left(\frac{R}{r}\right)\right\} + E_1 r \qquad (3)$$

where ϵ_a is a cut-off parameter and $2R$ is the diameter of a crystal containing one superlattice dislocation. The separation r of both unit dislocations is obtained by minimizing E_a in eqn. (3) with respect to r. In a similar way, E_b can be written as

$$E_b = 2A_\theta\left\{\ln\left(\frac{R}{\epsilon_b}\right) + \ln\left(\frac{R}{r-r_1}\right)\right\} + \\ + 2B_\theta\left\{\ln\left(\frac{R}{r_1}\right) + \ln\left(\frac{R}{r-r_1}\right)\right\} + \\ + E_1(r-2r_1) + 2(\gamma + E_2)r_1 \qquad (4)$$

where E_1 and E_2 are the APB energies outside and inside the stacking fault region respectively and γ is the stacking fault energy. The separations of the Shockley partials are obtained by minimizing E_b in eqn. (4) with respect to $r - r_1$ and r_1.

The separation of the Shockley partials (r, r_1) transforms to that in Fig. 1(a) by taking $r_1 = 0$. The coefficients A_θ, B_θ and C_θ are combinations of the energy factor and depend on the angle θ between the total Burgers vector and the dislocation line direction. Half the average separation between the superlattice dislocations can be substituted for the parameter R in eqns. (3) and (4). Using an E_{APB} in the range 50–100 mJ m^{-2}, E_a and E_b can be calculated for various values of R. It appears that the twofold dissociation of a screw superlattice dislocation requires less energy than the fourfold dissociation, whereas the opposite is valid for an edge superlattice dislocation.

This statement holds for a whole range of R values (0.1–1 μm) and for $\epsilon_a = b$ and $\epsilon_b = b_p$ where b represents the Burgers vector of a unit dislocation and b_p the Burgers vector of a Shockley partial. However, the dissociation scheme is very sensitive to the chosen values for the cut-off parameters ϵ_a and ϵ_b. When $\epsilon_a = \epsilon_b \approx b_p$, the fourfold dissociation is energetically more favourable than the twofold dissociation both for a screw and for an edge superlattice dislocation. Hence, it is rather difficult to predict the dissociation scheme for a superlattice dislocation in Cu_2NiZn *a priori*.

As already discussed in Section 3.1, a superlattice dislocation dipole consists of two superlattice dislocations of opposite signs on parallel glide planes. For simplicity we ignore the possible splitting of each unit dislocation into two Shockley partials separated by a complex stacking fault and hence the superlattice dislocation dipole can be characterized as illustrated in Fig. 3. In equilibrium the net force on each dislocation is equal to zero. Hence, for dislocation 1,

$$F_1 = \frac{\mu b^2}{2\pi}\left\{-\frac{1}{x_1} + \frac{x_0}{{x_0}^2 + {y_0}^2} + \right. \\ \left. + \frac{x_0 + x_1}{(x_0 + x_1)^2 + {y_0}^2}\right\} + E_1 - \tau_{xz} b \qquad (5)$$

and, for dislocation 2,

$$F_2 = \frac{\mu b^2}{2\pi}\left\{\frac{1}{x_1} + \frac{x_0 + x_1}{(x_0 + x_1)^2 + {y_0}^2} + \right. \\ \left. + \frac{x_0}{{x_0}^2 + {y_0}^2}\right\} - E_1 - \tau_{xz} b \qquad (6)$$

where τ_{xz} is a shear stress in the glide planes. Elimination of the term $\tau_{xz} b$ in eqns. (5) and (6) results in a relation between x_0 and x_1 for fixed values of y_0 and E_1. This relation is plotted for several y_0 values in Fig. 4, taking $E_1 = 40$ mJ m^{-2}. Each point on each curve corresponds to a different τ_{xz} value, which can be evaluated using eqn. (5) or eqn. (6).

To calculate the separations of the dislocations in the unstressed state, τ_{xz} must equal zero. From eqns. (5) and (6) it follows that this can be true only if $x_0 = 0$. This means that the two screw superlattice dislocations are right on top of each other. The larger y_0,

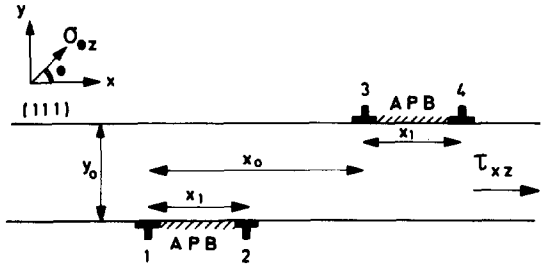

Fig. 3. Schematic illustration of the parameters characterizing a superlattice dislocation dipole.

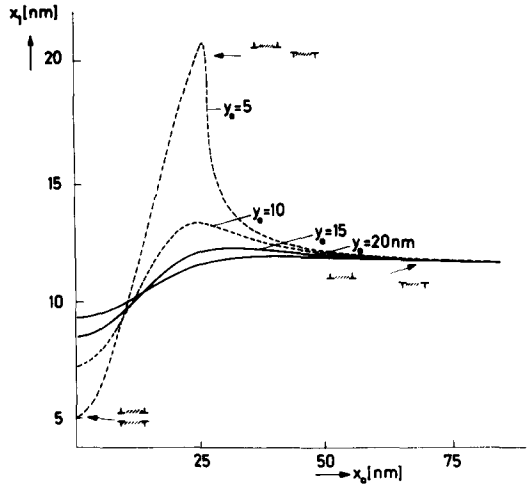

Fig. 4. The relation between the parameters characterizing the configuration of a screw superlattice dislocation dipole ($E_1 = 40$ mJ m^{-2}).

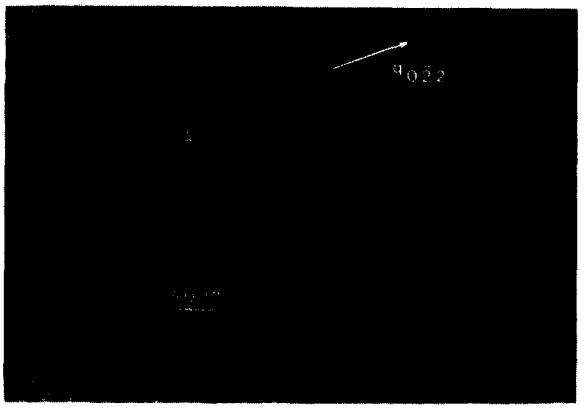

Fig. 5. Weak beam image of a superlattice dislocation dipole (at A) and two superlattice dislocations in a Cu_2NiZn single crystal annealed at 623 K for 164 h, deformed 13% in compression and annealed at 623 K for 75 min (the projection plane is the slip plane (111); $\boldsymbol{b} = \frac{1}{2}[0\bar{1}1]$; $\boldsymbol{g} = [0\bar{2}2]$; $s_g = +0.23$ nm^{-1}).

the larger x_1 will be, reaching asymptotically the configuration of two isolated superlattice dislocations.

3.3. *Experimental observations*

The superlattice dislocations are imaged in a dark field using the weak beam technique [12]. Identification of the slip plane is performed by observing the dislocation spacing on tilting the foil. Figure 5 shows a weak beam image of a superlattice dislocation dipole at A and two superlattice dislocations in a Cu_2NiZn single crystal. In order to determine the parameters characterizing the configuration of a superlattice dislocation dipole (Fig. 4), a few dipoles have been imaged in different projections to reconstruct the three-dimensional configuration. The observed separation of the imaged dislocation lines was obtained from a microdensitometer scan perpendicular to the dislocation line direction. The separation of the unit dislocations as a function of the character of the dislocations is depicted in Fig. 6 for the Cu_2NiZn alloy which has been annealed for 164 h at 623 K to obtain the $L1_2$ structure with a long-range order parameter S'' close to unity. The full curves in Fig. 6 are computed using anisotropic elasticity theory. An APB energy of 97 ± 17 mJ m^{-2} can be obtained for the unaged sample. This experimentally determined APB value agrees with the value of 85 mJ m^{-2} which can be computed from the ordering energies obtained from cohesive energy calculations [13]. Aging the sample after deformation results in a slight decrease in the APB energy and a substantial increase

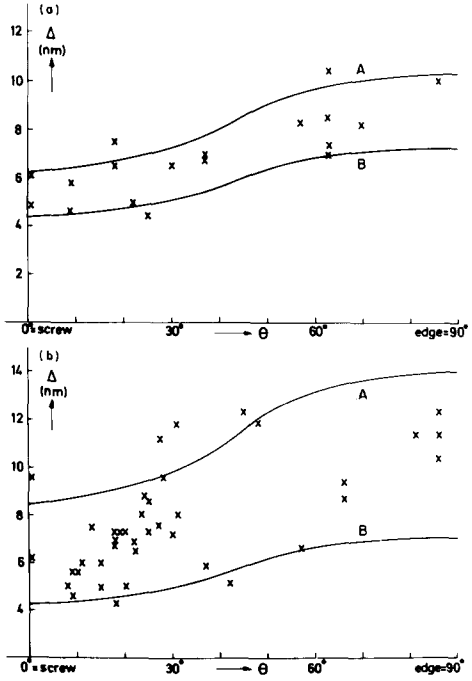

Fig. 6. Separation of the unit dislocation Δ as a function of the character θ of the dislocations in a Cu_2NiZn single crystal annealed for 164 h at 623 K, subsequently deformed to a strain of 13% and then (a) not annealed (curve A, $E_{APB} = 80$ mJ m^{-2}; curve B, $E_{APB} = 114$ mJ m^{-2}), (b) annealed for 75 min at 623 K (curve A, $E_{APB} = 59$ mJ m^{-2}; curve B, $E_{APB} = 117$ mJ m^{-2}): ——, results according to the anisotropic linear elasticity theory.

in the scatter of the observed separations. These features can be explained by the ongoing transformation of the discontinuous shear APB into the diffuse APB under thermal equilibrium, as described by Brown [14].

The parameters characterizing the configuration of the superlattice dislocation dipoles observed in Cu_2NiZn, as illustrated in Fig. 4, are compiled in Table 1. As can be concluded, there is only one configuration with $x_0 = 0$ and thus with a zero net force in the slip plane on the superlattice dislocation dipole. However, the APB energy obtained from the corresponding x_1 (and y_0) values is rather small, *i.e.* about 33 mJ m^{-2}. APB energies deduced from eqns. (5) and (6) using values for the parameters quoted in Table 1 are in the range from 20 to 35 mJ m^{-2}, which is much smaller than the value of the APB energy determined from the separation of the unit dislocations in a superlattice dislocation. Only one superlattice dislocation dipole ($\theta = 15°$) resulted in a reasonable value for the APB energy, which yielded 96 mJ m^{-2}.

Internal shear stresses τ_{xz} deduced from eqns. (5) and (6) range from 10 to 200 MPa. The latter is very high, bearing in mind that the critical resolved shear stress for Cu_2NiZn is about 40 MPa and that stress fields of superlattice dislocation dipoles are only important at short distances (the net Burgers vector is zero). Hence the values of the APB energy and internal stresses determined from the configuration of superlattice dislocation dipoles in Cu_2NiZn are not very reliable.

So far, we have considered superlattice dislocations in a completely $L1_2$ ordered structure. According to Fisher [15], the work required to move a unit dislocation is

$$\tau b = E_f - E_i \tag{7}$$

where τ is the shear stress, and E_f is the final and E_i the initial energy per unit slip plane area due to bonding across the slip plane. For the $L1_2$ structure of Cu_2NiZn, eqn. (7) becomes

$$\tau b = \frac{1}{2a_0{}^2 3^{1/2}}\left\{-\frac{1}{3}(S''^2 - 9\alpha_{CuNi})W_{CuNi} + \right.$$
$$+ (S''^2 + 3\alpha_{CuZn})W_{CuZn} +$$
$$\left. + \frac{1}{2}(S''^2 + 3\alpha_{NiZn})W_{NiZn}\right\} \tag{8}$$

where α_{ij} represents the Cowley short-range order parameter, W_{ij} the ordering energy and a_0 the lattice parameter. Usually it is assumed that the short-range order correlation across the slip plane is destroyed after the passage of one dislocation [16]. Consequently, for Cu_2NiZn quenched from above the critical temperature for ordering ($S'' = 0$) and therefore containing only α_{ij} values, it would be expected that the short-range order is destroyed after the passage of a single dislocation. However, we observed that the short-range order is destroyed after the passage of about seven superlattice dislocations as is shown in Fig. 7. The sequential dislocation pairing with increasing pair spacing can be ascribed to shear induced oscillations in short range order [24].

With respect to the dislocation reaction in the nickel-base superalloy containing $L1_2$ ordered precipitates, three modes of deformation are to be expected: as well as the glide of $\frac{1}{2}\langle 110\rangle$ single dislocations in the disordered matrix, the localized shearing on

TABLE 1

Parameter characterizing the configuration of a superlattice dislocation dipole

b	θ (deg)	*Slip plane*	x_0 (nm)	x_1 (nm)	y_0 (nm)	T (K)
$\frac{1}{2}[01\bar{1}]$	36	$(\bar{1}11)$	7	22	22	623
$\frac{1}{2}[01\bar{1}]$	10	(111)	8	20	25	623
			2	10	6	623
$\frac{1}{2}[01\bar{1}]$	15	(111)	19	5	1	623
$\frac{1}{2}[1\bar{1}0]$	60	$(11\bar{1})$	0	11	19	623
$\frac{1}{2}[1\bar{1}0]$	67	$(11\bar{1})$	15	13	15	623
$\frac{1}{2}[01\bar{1}]$	44	$(\bar{1}11)$	28	21	39	763

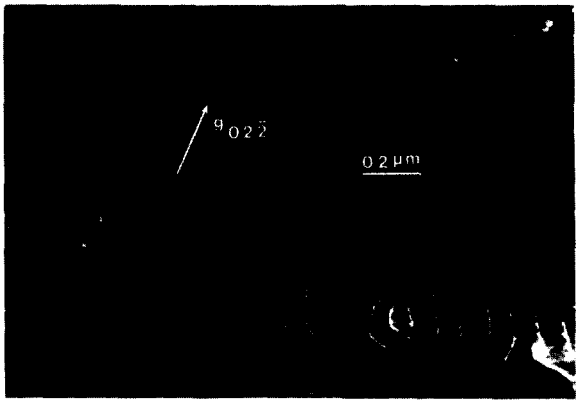

Fig. 7. Weak beam dark field image of a pile-up in polycrystalline Cu_2NiZn quenched from 835 K and deformed 5% in tension (projection plane, (111); $b = \frac{1}{2}a_0[10\bar{1}]$; $g = [02\bar{2}]$; $s_g = 0.10\ nm^{-1}$).

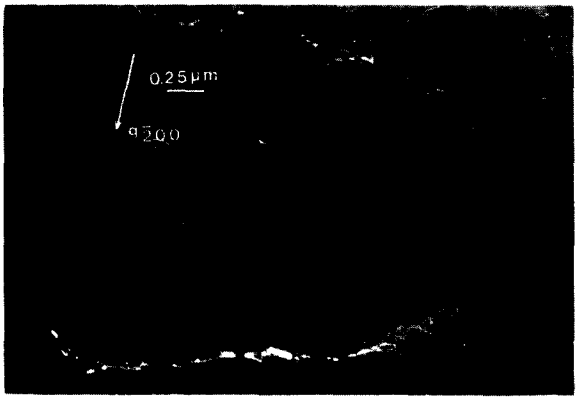

Fig. 8. Dark field, weak beam image of a superlattice screw dislocation ($\dot{\epsilon} = 10^{-2}\ s^{-1}$; $\Delta\epsilon_p = 10^{-4}$ at 1003 K) in a nickel-base superalloy.

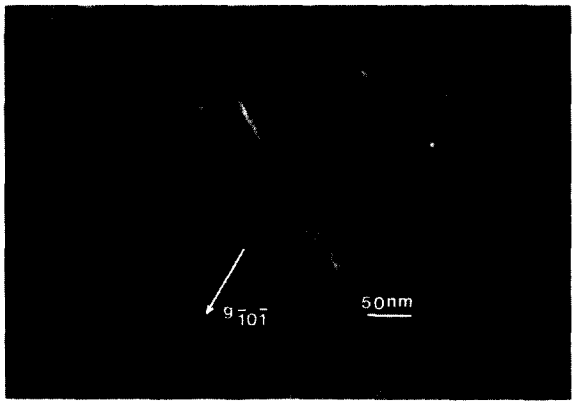

Fig. 9. $\frac{1}{3}\langle 112\rangle$ superlattice dislocation ($\dot{\epsilon} = 10^{-6}\ s^{-1}$; $\Delta\epsilon_p = 10^{-4}$ at 1003 K).

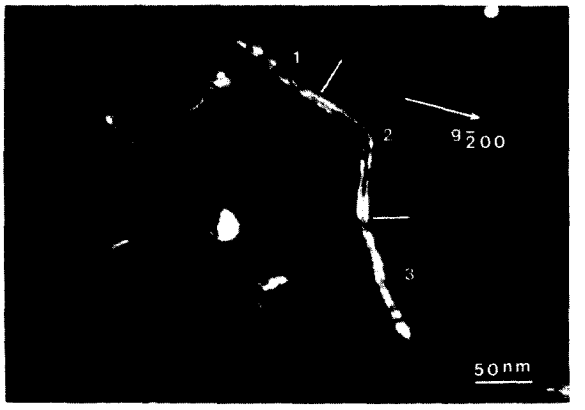

Fig. 10. Dark field, weak beam image of a $\frac{1}{2}\langle 110\rangle$ superlattice dislocation ($\dot{\epsilon} = 5 \times 10^{-5} s^{-1}$; low cycle fatigue testing at 1003 K; $\Delta\epsilon_p = 3 \times 10^{-4}$).

{111} planes caused by $\frac{1}{3}\langle 112\rangle$ super Shockley partials (Fig. 1(c)) and the cutting of γ' precipitates by pairs of $\frac{1}{2}\langle 110\rangle$ super unit dislocations (Fig. 1(a)). Figure 8 shows a large γ' particle containing $\frac{1}{2}\langle 110\rangle$ super pairs. The super partials $\frac{1}{3}\langle 112\rangle$ form the more dominant mode of deformation while occasionally in a large γ' a $\frac{1}{2}\langle 110\rangle$ superdislocation pair was found (Fig. 9). At high temperatures, thermal vacancies facilitate $\frac{1}{3}\langle 112\rangle$-type shear of γ' precipitates. The vacancies provide a geometrically necessary dipole displacement at the core of each $\frac{1}{3}\langle 112\rangle$ super partial. Consequently, the γ' particles can be sheared without dislocation constrictions at the γ'–matrix interface [17]. The $\frac{1}{2}\langle 110\rangle$ superdislocations are possible when the ordering energy is sufficiently low, thus at higher temperatures keeping the strain rate high. At high temperatures the effective APB energy is decreased because of interactions with thermal vacancies. As a result the paired $\frac{1}{2}\langle 110\rangle$ dislocations can be resolved separately by TEM (Fig. 8).

Occasionally, at high temperatures the super pairs show up in typical N-shaped configurations (Fig. 10). Detailed investigation, using extinction criteria and edge-on imaging, revealed that the beginning and end sections of the N are of a screw nature gliding on {111} planes while the section in between lies on a cubic plane. On the basis of stereo-TEM observations [22], Fig. 10 can best be interpreted by assuming a glissile part on $(1\bar{1}1)$, a cross-slipped part on (001) oriented along [010] and a part which has climbed towards $(\bar{1}\bar{1}1)$. These three main sections are

indicated separately in Fig. 10. The reaction is that of a double-cross-slip mechanism, plausibly due to constriction-dissociation of the super pairs at the γ'-γ interface. Unfortunately, the γ' precipitates could not be visualized at all because of heavy deformation. The superlattice (100) and (110) spot had hardly any intensity left. It is physically plausible that the configuration of the superlattice dislocation is strongly influenced by the sheared γ' particles. Nevertheless we measured the distance d between the dislocations on $(1\bar{1}1)$ determined from Fig. 10 to be 3.5 nm. The formula

$$E_{APB} = K\frac{\mu b^2}{2\pi d}$$

with $K = 1$ for a screw dislocation, $\mu = 66.66$ GPa and $|b| = 0.25$ nm results in $E_{APB}\{111\} = 189$ mJ m^{-2}. For the parts in an edge orientation on {100}, a dissociation of 9.1 nm at maximum (Fig. 10) is found, leading to an APB energy on {100} of 104 mJ m^{-2}. It should be emphasized that these are extreme values since internal stresses might change the values obtained for the APB considerably. For instance, recently, Veyssière [18] reported a value of 140 mJ m^{-2} for the APB energy on {100} in polycrystalline Ni_3Al. Although the separations of the superlattice dislocation may be affected by these stresses, the influence is assumed to be smaller when the ratio of the APB energy on {111} to that on {100} is considered:

$$\frac{E_{\{100\}}}{E_{\{111\}}} = -\frac{W^{(2)}3^{1/2}}{W^{(1)}} = 0.55$$

where $W^{(i)}$ represents the ordering energy at the ith nearest neighbouring distance. This ratio together with the experimental findings that $W^{(1)} < 0$ and $W^{(2)} > 0$ predict a stable $L1_2$ structure [19, 20].

The observations (Fig. 10) suggest that a continuous transition from $(1\bar{1}1)$ to (001) occurs. Our findings in $L1_2$ precipitation-strengthened material are analogous to the experimental results obtained by Veyssière [18] and Veyssière *et al.* [21] in polycrystalline Ni_3Al as far as the climb process towards {001} is concerned. It is not clear yet whether this temperature strengthening process due to climb dissociation plays an important role in the mechanical behaviour of the superalloy under investigation.

4. CONCLUSIONS

Possible configurations of dislocations in the $L1_2$ ordered alloy Cu_2NiZn and in the nickel-base superalloy containing $L1_2$ ordered precipitates have been investigated. From the observed distances between ⟨110⟩ superlattice dislocation, values of the APB energy have been calculated. Twofold dissociation of a superlattice dislocation in Cu_2NiZn is more likely than fourfold dissociation, provided that the complex stacking fault energy is about the sum of the APB energy and the stacking fault energy. Superlattice dislocation dipoles are not very reliable for the determination of the APB energy and probably also not for the determination of internal stresses. In Cu_2NiZn quenched from above the critical temperature for ordering, the short-range order is destroyed after the passage of about seven superlattice dislocations instead of one single dislocation. In the superalloy under investigation, both $\frac{1}{2}$⟨110⟩ superlattice dislocations and $\frac{1}{3}$⟨112⟩ dislocation pairs are observed, indicating that the superlattice intrinsic stacking fault energy is comparable with the APB energy. In addition to {111} cross-slip behaviour, temperature strengthening due to climb dissociation onto {100} has been observed.

ACKNOWLEDGMENTS

The work is part of the research programme of the Foundation for Fundamental Research on Matter (FOM, Utrecht) and has been made possible by financial support from The Netherlands Organization for the Advancement of Pure Research (ZWO, The Hague).

REFERENCES

1 J. S. Koehler and F. Seitz, *J. Appl. Mech.*, *14* (1947) 217.
2 U. Dehlinger and L. Graf, *Z. Phys.*, *64* (1930) 359.
3 S. Ogawa, D. Watanabe, H. Watanabe and T. Komoda, *Acta Crystallogr.*, *11* (1958) 872.
4 M. J. Marcinkowski, R. M. Fisher and N. Brown, *J. Appl. Phys.*, *31* (1960) 1303.
5 J. Th. M. De Hosson, in T. Tsakalakos (ed.), *Order–Disorder Transformations*, Elsevier,

Amsterdam, 1984, p. 277.
6 G. J. L. van der Wegen, R. Helmholdt, P. M. Bronsveld and J. Th. M. De Hosson, *Z. Metallkund., 74* (1983) 592.
7 G. J. L. van der Wegen, P. M. Bronsveld and J. Th. M. De Hosson, *Philos. Mag. A, 47* (1983) 193.
8 M. Yamaguchi, V. Paidar, D. P. Pope and V. Vitek, *Philos. Mag. A, 45* (1982) 867.
9 K. Suzuki, M. Ichihara and S. Takeuchi, *Acta Metall., 27* (1979) 193.
10 J. de Groot, P. M. Bronsveld and J. Th. M. De Hosson, *Phys. Status Solidi A, 52* (1979) 635.
11 G. J. L. van der Wegen, P. M. Bronsveld and J. Th. M. De Hosson, *Metall. Trans. A, 11* (1980) 1125.
12 D. J. H. Cockayne, *Z. Naturforsch., 27a* (1972) 452.
13 J. Th. M. De Hosson, in J. K. Lee (ed.), *Interatomic Potentials and Crystalline Defects*, Metallurgical Society of AIME, Warrendale, PA, 1981, pp. 3–31.
14 N. Brown, *Philos. Mag., 4* (1959) 693.
15 J. C. Fisher, *Acta Metall., 2* (1954) 9.
16 P. S. Rudman, *Acta Metall., 10* (1962) 253.
17 J. M. Oblak and B. Kear, in G. Thomas (ed.), *Electron Microscopy and Structure of Materials*, University of California Press, Berkeley, CA, 1972, p. 566.
18 P. Veyssière, *Philos. Mag., 50* (1984) 189.
19 J. Kanamori, *Prog. Theor. Phys., 35* (1966) 16.
20 S. M. Allen and J. W. Cahn, *Acta Metall., 20* (1972) 423.
21 P. Veyssière, D. L. Guan and J. Rabies, *Phil. Mag., 49* (1984) 45.
21 P. Veyssière, D. L. Guan and J. Rabies, *Philos. Mag., 49* (1984) 45.
22 A. Huis in 't Veld, G. Boom, P. M. Bromsveld and J. Th. M. De Hosson, *Scripta Metall., 19* (1985) 105.
23 A. E. Vidoz and L. M. Brown, *Philos. Mag., 7* (1962) 1167.
24 J. B. Cohen and M. E. Fine, *J. Phys. Radium, 23* (1962) 749.